

Electrical conductivity for warm, dense aluminum plasmas and liquids

M. P. Desjarlais,^{1,*} J. D. Kress,² and L. A. Collins²

¹*Pulsed Power Sciences Center, Sandia National Laboratories, Albuquerque, New Mexico 87185*

²*Theoretical Division, Los Alamos National Laboratory, Los Alamos, New Mexico 87545*

(Received 28 February 2002; published 26 August 2002)

The electrical conductivity of warm, dense aluminum plasmas and liquids is calculated using *ab initio* molecular dynamics and the Kubo-Greenwood formula. The density range extends from near solid to one-hundredth of solid density, and the temperature range extends from 6000 K to 30 000 K. This density and temperature range allows direct comparison with experimental results obtained with the tamped exploding wire technique.

DOI: 10.1103/PhysRevE.66.025401

PACS number(s): 52.25.Fi, 52.27.Gr, 52.80.Qj, 72.15.-v

A particularly fruitful area for the study of metals is their evolution through various phases with associated transitions in the electrical properties. Such environments, as alkali metals around the liquid-vapor coexistence boundary [1] and tamped wires exploded by an intense electrical current [2–4], provide but two important examples. The results of such examinations have profound ramifications to a diverse set of fields: materials modeling, plasma characterization and production, and systems under extreme conditions, for example, planetary interiors. In the case of high-energy density physics experiments employing exploding wires, the material moves from a solid, through a liquid, to a plasma state. Most of the complexity appears in the first two decades of decreasing density below solid, and for temperatures up to a few eV. Since this experimental data is only obtained along the trajectory in density and temperature space that the wire traces as it explodes, practical limits exist to the completeness of the experimental data. In addition, in many of these experiments, the temperature is not measured directly, but rather, inferred through auxiliary equations of state and simulations, leading to some additional uncertainty in the results. In this paper, we use a combination of *ab initio* molecular dynamics and a first principles conductivity calculation to examine the conductivity in this regime. This serves as a very useful comparison with the experimental measurements, permits an extension into densities and temperatures not covered by the experiments, and provides insight into the underlying physics.

Ion configurations for the conductivity calculation are obtained by performing *ab initio* molecular dynamics (MD) simulations within the framework of the finite temperature density functional theory (FT-DFT) of Mermin [5]. These MD calculations are performed using VASP (Vienna *ab initio* simulation program), a plane-wave density functional code developed at the Technical University of Vienna [6–9]. For the MD runs, the ions and their respective core wave functions are modeled using the Vanderbilt [10] ultrasoft pseudopotentials (US-PP) supplied with VASP [11]. These ultrasoft pseudopotentials significantly reduce the computational effort, particularly for large supercells. The DFT exchange and correlation functionals are calculated at the level of both the

local density and generalized gradient (GGA) approximations, the latter using the parametrization of Perdew-Wang 91 [12], with the plane wave cutoff (E_{cut}) at 129 eV. The bulk of the MD calculations were carried out using only the Γ point for representation of the Brillouin zone (BZ). Several (ρ, T) pairs were also examined with higher-order \mathbf{k} -point sets, such as the Monkhorst-Pack $2 \times 2 \times 2$ [13], or the Baldereschi mean value point [14], but with no significant effect on the corresponding conductivity calculation.

Following the molecular dynamics simulation, a total of ten to twenty configurations are selected from an equilibrated (in an average sense) portion of the molecular dynamics run, typically sampling the final picosecond of evolution. For each of these configurations, the electrical conductivity is calculated using the Kubo-Greenwood formula [15–17]. For these static configuration calculations, VASP is run in the GGA with $E_{\text{cut}} = 180$ eV, using the projector augmented wave (PAW) potentials [18,19]. The PAW potentials provide a significant advantage over the US-PP in applying the Kubo-Greenwood formula since the all electron PAW treatment avoids the complication of calculating an awkward correction term related to the nonlocal pseudopotential operator.

The Kubo-Greenwood (KG) formula is a general expression for the conductivity, and includes electron-atom, electron-ion, and electron-electron interactions. Since the KG formula calculates the conductivity directly from the electronic wave function, one avoids the difficulties of calculating or modeling, independently and consistently, the population of free electrons, the various relaxation times between the electrons and other species, and the proper form of the pseudopotential and screening model. While this latter approach has proven quite successful at lower densities where the Debye screening model applies [20,21] difficulties have been noted in the dense plasma limit where stronger coupling occurs and the Debye screening model becomes a poor approximation [21].

The Kubo-Greenwood formula for the electrical conductivity as a function of the frequency ω (also referred to as the optical conductivity) for a particular \mathbf{k} point in the Brillouin zone of the simulation supercell may be written

$$\sigma_{\mathbf{k}}(\omega) = \frac{2\pi e^2 \hbar^2}{3m^2 \omega \Omega} \sum_{j=1}^N \sum_{i=1}^N \sum_{\alpha=1}^3 [F(\epsilon_{i,\mathbf{k}}) - F(\epsilon_{j,\mathbf{k}})] \times |\langle \Psi_{j,\mathbf{k}} | \nabla_{\alpha} | \Psi_{i,\mathbf{k}} \rangle|^2 \delta(\epsilon_{j,\mathbf{k}} - \epsilon_{i,\mathbf{k}} - \hbar \omega), \quad (1)$$

*Electronic address: mpdesja@sandia.gov

where e and m are the electron charge and mass. The i and j summations are over the N discrete bands included in the triply periodic calculation for the cubic supercell volume element Ω . The α sum is over the three spatial directions and improves the statistics. $F(\epsilon_{i,\mathbf{k}})$ is the Fermi weight corresponding to the energy $\epsilon_{i,\mathbf{k}}$ for the i th band at \mathbf{k} ; $\Psi_{i,\mathbf{k}}$ is the corresponding wave function. In practice, because of the finite simulation volume and resulting discrete eigenvalues, the δ function must be broadened; we use a Gaussian broadening of the δ function that is taken to be as small as feasible without recovering the local oscillations in the optical conductivity resulting from the discrete band structure. A good initial starting point for the width of the Gaussian is the average of the nearest neighbor change in the eigenvalues, weighted by the corresponding change in the Fermi function. In general, the integration over the Brillouin zone is performed using the method of special \mathbf{k} points [13,14],

$$\sigma(\omega) = \sum_{\mathbf{k}} \sigma_{\mathbf{k}}(\omega) W(\mathbf{k}), \quad (2)$$

where $W(\mathbf{k})$ is the weighting factor for the point \mathbf{k} in the Brillouin zone. Finally, the average of $\sigma(\omega)$ is taken over the ensemble of configurations sampled. The dc electrical conductivity is given by $\sigma_0 \equiv \sigma(0)$.

We examine a range of densities from 0.025 to 2.0 g/cm³. For densities of 1.0 to 2.0 g/cm³, the simulations were done with 108 atoms in the supercell. Because of computational limitations, it was necessary to drop the number of atoms N_a as the size of the supercell increased. For densities from 0.05 g/cm³ up to 1.0 g/cm³, we used 32 atoms per supercell. For 0.05 and 0.1 g/cm³, we performed simulations with 16 atoms per supercell, and dropped to as few as eight atoms in the supercell at the lowest density 0.025 g/cm³. At each reduction in N_a , comparisons were made between two supercells, say 16 and 32 atoms, at the same physical density, to rule out significant differences due to the number of atoms in the supercell. In all cases these differences were within 10%.

An important and useful check on the consistency of the optical conductivity calculation is the well-known sum rule [17]

$$S \equiv \frac{2m\Omega}{\pi e^2 N_e} \int_0^\infty \sigma(\omega) d\omega = 1, \quad (3)$$

where N_e is the number of electrons in the supercell volume Ω —three valence electrons per atom for the specific Al-PAW potentials used here. In general, since the low-frequency part of $\sigma(\omega)$ converges with increasing number of bands much faster than the high-frequency tail, the dc conductivity converges well before the sum rule. We maintained a sufficient number of bands to satisfy the sum rules to at least within 7%, and typically much better (2%), which means the dc conductivities are converged to an even higher degree. In addition, we obtain highly accurate values of $\sigma(\omega)$ by sampling between 10 and 20 well separated MD steps.

The results of the DFT-MD, Kubo-Greenwood calculations are shown in Fig. 1 for densities from near solid, down

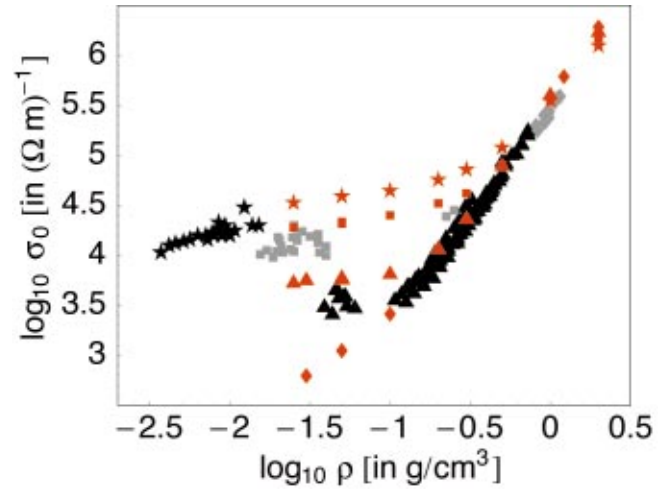


FIG. 1. (Color) Aluminum dc electrical conductivity versus density for data and calculations at 6 kK (diamonds), 10 kK (triangles), 20 kK (squares), and 30 kK (stars). Calculation results are in red; the data from the experiments of DeSilva and Katsouros are in gray (6 and 20 kK) and black (10 and 30 kK).

to about one hundredth of solid (0.025 g/cm³), and for temperatures of 6, 10, 20, and 30 kK, corresponding to data sets from DeSilva and Katsouros [2]. Examination of the dynamical properties, such as the self-diffusion coefficient, indicates that the system moves from a liquid to a near vapor (ionized) over this density regime. The agreement between the simulations and the data is very good and holds up well over the two decades of density variation.

There are several interesting features of the conductivity behavior as a function of density and temperature. For a given temperature, there is a density above which the conductivity effectively merges with a limiting envelope of the conductivity isotherms. However, the density at which this occurs does depend on temperature. Examining the band structure and corresponding optical conductivity as the density is lowered from the dense liquid limit, we find that the dc conductivity departs from the limiting envelope at the density at which a gap (or pseudogap) separating the 3s and 3p levels forms about the Fermi energy. This gap forms at higher densities for higher temperatures. Thus one finds that for lower temperatures the conductivities trace the envelope to lower densities before breaking off. This behavior is consistent with the experimental results and is also seen in partially ionized plasma (PIP) calculations [20,21]. For densities above this critical density for a given temperature, the dc conductivities are very weakly dependent on the temperature, but are strongly dependent on the density; σ_0 scales approximately as $\rho^{7/3}$. As the density drops significantly below the transition density, the gap at the Fermi energy broadens and the dc conductivity results mostly from the tail of the Fermi distribution above the gap. This effect is increased further with the higher temperatures and lower densities, because of the increased Fermi broadening and increased density of states, respectively. Proper resolution of this tail can require a very large number of bands in the simulation; as many as 2000 bands for the 20 and 30 kK cases may be necessary for convergence of the dc conductivity at the low-

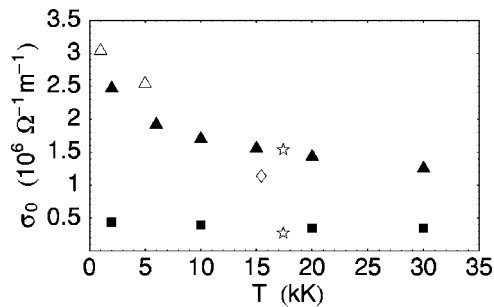


FIG. 2. Aluminum dc electrical conductivity versus temperature at 1 g/cm^3 (squares) and 2 g/cm^3 (triangles). Also shown for 2 g/cm^3 are MD-KG results from Ref. [22] (open triangles), an experimental data point from Ref. [4] (open diamond), and for both 1 and 2 g/cm^3 , the average-atom DFT results of Ref. [23] (stars).

est densities shown. Fortunately, in this limit, the results are not sensitive to the choice of \mathbf{k} points, and it has been proven sufficient to use only the Γ point, $\mathbf{k}=(0,0,0)$, which, through the symmetry, significantly reduces the computational effort.

The largest differences between the calculations and the data appear at lower temperatures and densities, where the sensitivity to the temperature is greatest and the results are within the error bars for the inferred temperature. However, because the dc conductivity in this limit results from the Fermi tail above the gap that forms at the Fermi energy, another possible cause for this difference merits discussion. It is well known that DFT underestimates the size of the band gap in insulators and semiconductors with varying degree depending on the material. This phenomenon could have a systematic effect on the calculated dc conductivities at low densities. However, we expect this effect to be small because gap corrections at the level of a “scissors” operator do not significantly change the contribution of adjacent bands to the dc conductivity in this limit.

It is also evident from Fig. 1 that there is, for the temperature range considered here, a qualitative change in the scaling of the dc conductivity with temperature at a density of about 1.0 g/cm^3 . For densities above this value, the conductivity is inversely proportional to temperature, similar to the well-known behavior for the solid. This is illustrated more clearly in Fig. 2 that shows the behavior of the conductivity with temperature at both 1.0 g/cm^3 (squares) and 2.0 g/cm^3 (triangles). At 1.0 g/cm^3 , the conductivity shows almost no variation with temperature in this range. Also shown, for comparison to the 2.0 g/cm^3 results are the results of similar MD-KG calculations by Silvestrelli [22] (open triangles), and an experimental data point from Benage *et al.* [4] (open diamond) obtained from measurements of exploding wires tamped with lead glass. Our results are in good agreement with both, lying somewhat in between. The open stars show two results for 17.4 kK (1.5 eV) from the average atom DFT approach of Perrot and Dharma-wardana [23] based on the extended Ziman formula for the conductivity [24]; the lower star is for 1.0 g/cm^3 , the upper for 2.0 g/cm^3 . The extrapolated agreement is within a few percent for the upper point and about 30% for the lower point.

The character of the optical conductivity changes dramatically over the density range examined here. In Fig. 3 we

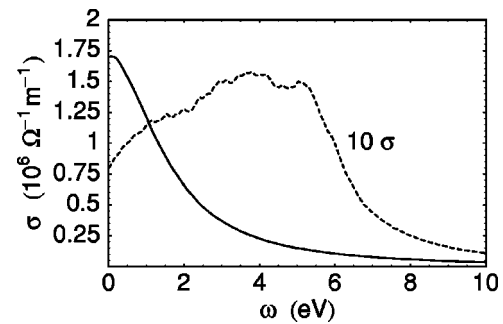


FIG. 3. The aluminum optical conductivity versus ω at 2 g/cm^3 and 10 kK (solid line) and for 0.5 g/cm^3 and 20 kK (scaled by 10, dashed line).

show the optical conductivity $\sigma(\omega)$ in units of eV for a density of 2 g/cm^3 , and a temperature of 10 kK (solid line). For these conditions, a Drude fit to the optical conductivity $\sigma = \sigma_0 / (1 + \omega^2 \tau^2)$ is almost indistinguishable from the plot, indicating the nearly-free-electron nature of the system. This is typical of the higher densities.

For a range of intermediate densities, the optical conductivity shows no Drude character at low frequencies. The dashed line in Fig. 3 shows $10 \sigma(\omega)$ (to use the same scale) for a density of 0.5 g/cm^3 and a temperature of 20 kK . At this density and temperature a pseudogap is just beginning to form at the Fermi energy with lowering density and the optical conductivity peaks near 4 eV .

At the lower densities investigated here, there is a reemergence of a Drude-like component in the low-energy optical conductivity. This is illustrated in Fig. 4 for a density of 0.025 g/cm^3 and a temperature of 30 kK . The prominent peak at 5.8 eV is characteristic of the $3s \rightarrow 3p$ transition for an isolated aluminum atom. The optical conductivity is well fit by the Drude formula out to about 0.5 eV (dashed line). One can use the Drude fit to the optical conductivity with $\sigma_0 = n_e e^2 \tau / m$ to estimate the effective conduction electron density n_e . For the example shown in Fig. 4, this gives an effective average $\bar{Z} \equiv n_e \Omega / N_a$ of 0.88 . This is in reasonably good agreement with the PIP calculation of Redmer [20], where a value of ~ 1.15 was obtained for the same conditions. Examination of the states and band structure indicates that the Drude-like conductivity behavior seen here comes

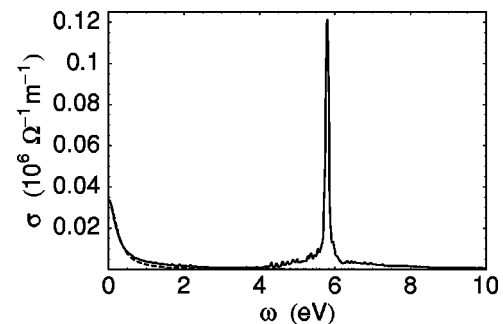


FIG. 4. The aluminum optical conductivity versus ω at 0.025 g/cm^3 and 30 kK . The Drude fit to the lower energies is shown with the dashed line.

almost entirely from those states far out on the tail of the Fermi distribution. As mentioned above, this requires a very large number of bands, 2000 in this case, to obtain convergence on the dc conductivity. This finding is consistent with the medium beginning to form a fully ionized plasma with the electrons now occupying the high-lying continuum states of the system. That a condensed matter approach can represent the basic characteristics of a diffuse plasma augurs well for the systematic treatment of diverse states of matter.

The dc electrical conductivities obtained from the *ab initio* MD-KG simulations presented here give good agreement with the data obtained in tamped exploding wire experiments and demonstrate a useful tool for expanding on, and providing additional corroboration to, the experimental results over a broad range of density and temperature conditions. These

new conductivity results have proven extremely useful in improving our conductivity modeling algorithms [25] and tables for use in simulation codes and have allowed dramatic improvement in simulations of exploding wires [26] and magnetically launched flyer plates [27].

We gratefully acknowledge useful discussions with Alan DeSilva, Stephane Mazevet, Ronald Redmer, and Sandra Kuhlbrodt. Sandia is a multiprogram laboratory operated by Sandia Corporation, a Lockheed Martin Company, for the United States Department of Energy under Contract No. DE-AC04-94AL85000. The work of J. D. Kress and L. A. Collins was performed under the auspices of the United States Department of Energy through the Theoretical Division of Los Alamos National Laboratory.

-
- [1] S.R. Bickham *et al.*, Phys. Rev. B **58**, 11 813 (1998).
 - [2] A.W. DeSilva and J.D. Katsourous, Phys. Rev. E **57**, 5945 (1998).
 - [3] I. Krisch and H.-J. Kunze, Phys. Rev. E **58**, 6557 (1998).
 - [4] J.F. Benage, W.R. Shanahan, and M.S. Murillo, Phys. Rev. Lett. **83**, 2953 (1999).
 - [5] N.D. Mermin, Phys. Rev. **137**, A1441 (1965).
 - [6] G. Kresse and J. Hafner, Phys. Rev. B **47**, 558 (1993).
 - [7] G. Kresse and J. Hafner, Phys. Rev. B **49**, 14 251 (1994).
 - [8] G. Kresse and J. Furthmüller, Comput. Mater. Sci. **6**, 15 (1996).
 - [9] G. Kresse and J. Furthmüller, Phys. Rev. B **54**, 11 169 (1996).
 - [10] D. Vanderbilt, Phys. Rev. B **41**, 7892 (1990).
 - [11] G. Kresse and J. Hafner, J. Phys.: Condens. Matter **6**, 8245 (1994).
 - [12] Y. Wang and J.P. Perdew, Phys. Rev. B **44**, 13 298 (1991).
 - [13] H.J. Monkhorst and J.D. Pack, Phys. Rev. B **13**, 5188 (1976).
 - [14] A. Baldereschi, Phys. Rev. B **7**, 5215 (1973).
 - [15] R. Kubo, J. Phys. Soc. Jpn. **12**, 570 (1957).
 - [16] W. A. Harrison, *Solid State Theory* (McGraw-Hill, New York, 1970).
 - [17] G.D. Mahan, *Many Particle Physics* (Plenum Press, New York, 1981).
 - [18] P.E. Blöchl, Phys. Rev. B **50**, 17 953 (1994).
 - [19] G. Kresse and J. Joubert, Phys. Rev. B **59**, 1758 (1999).
 - [20] R. Redmer, Phys. Rev. E **59**, 1073 (1999).
 - [21] S. Kuhlbrodt and R. Redmer, Phys. Rev. E **62**, 7191 (2000).
 - [22] P.L. Silvestrelli, Phys. Rev. B **60**, 16 382 (1999).
 - [23] F. Perrot and M.W.C. Dharma-wardana, Phys. Rev. E **52**, 5352 (1995).
 - [24] R. Evans *et al.*, in *Properties of Liquid Metals*, edited by S. Takeuchi (Wiley, New York, 1973).
 - [25] M.P. Desjarlais, Contrib. Plasma Phys. **41**, 267 (2001).
 - [26] S.E. Rosenthal, M.P. Desjarlais, and K.R. Cochrane, Bull. Am. Phys. Soc. **46**(8), 28 (2001).
 - [27] R.W. Lemke *et al.*, Bull. Am. Phys. Soc. **46**(4), 21 (2001).